Long-range electron transport in *Geobacter sulfurreducens* biofilms is redox gradient-driven

Rachel M. Snider[a], Sarah M. Strycharz-Glaven[b], Stanislav D. Tsoi[b], Jeffrey S. Erickson[b], and Leonard M. Tender[b,1]

[a]National Research Council, Washington, DC 20001; and [b]Center for Bio/Molecular Science and Engineering, Naval Research Laboratory, Washington, DC 20375

Geobacter spp. can acquire energy by coupling intracellular oxidation of organic matter with extracellular electron transfer to an anode (an electrode poised at a metabolically oxidizing potential), forming a biofilm extending many cell lengths away from the anode surface. It has been proposed that long-range electron transport in such biofilms occurs through a network of bound redox cofactors, thought to involve extracellular matrix *c*-type cytochromes, as occurs for polymers containing discrete redox moieties. Here, we report measurements of electron transport in actively respiring *Geobacter sulfurreducens* wild type biofilms using interdigitated microelectrode arrays. Measurements when one electrode is used as an anode and the other electrode is used to monitor redox status of the biofilm 15 µm away indicate the presence of an intrabiofilm redox gradient, in which the concentration of electrons residing within the proposed redox cofactor network is higher farther from the anode surface. The magnitude of the redox gradient seems to correlate with current, which is consistent with electron transport from cells in the biofilm to the anode, where electrons effectively diffuse from areas of high to low concentration, hopping between redox cofactors. Comparison with gate measurements, when one electrode is used as an electron source and the other electrode is used as an electron drain, suggests that there are multiple types of redox cofactors in *Geobacter* biofilms spanning a range in oxidation potential that can engage in electron transport. The majority of these redox cofactors, however, seem to have oxidation potentials too negative to be involved in electron transport when acetate is the electron source.

microbial fuel cell | bioelectrochemical system | microbial electrochemistry | geomicrobiology | multistep electron hopping

It is widely accepted that electron transport can occur over molecular-scale distances in biological systems by electron hopping among a small number of immobilized redox cofactors (1, 2). There is growing awareness, however, of the possibility of electron transport over length scales much longer than previously thought possible in biological systems by using immobilized redox cofactors organized into electron transport conduits. This is most evident by microorganisms, such as *Shewanella* spp. and *Geobacter* spp., that can use electron acceptors residing outside the cell for respiration (3). For example, in the case of *Shewanella*, it is proposed that the CymA-MtrA-MtrC complex comprised of 3 multiheme *c*-type cytochromes totaling 24 hemes acts as a multistep conduit that conducts respired electrons originating in the cytoplasm from the inner membrane through the periplasm and outer membrane to the cell outer surface (4–6). Outside the cell, both *Shewanella* and *Geobacter* secrete nanometer scale diameter, micrometer scale long proteinaceous filaments, referred to as pili and microbial nanowires (7), that extend from their outer surfaces into the extracellular matrix (ECM) thought to be involved in extracellular electron transport processes, including cell-to-cell electron transfer (8) and reduction of insoluble oxidants (9). Ex situ conductivity measurements of individual filaments of *Shewanella oneidensis* MR-1 confirm their lengthwise conductivity when isolated from cells under specific conditions (10, 11), and subsequent modeling of their current–voltage characteristics is consistent with multistep electron hopping involving redox cofactors proposed to be associated with these filaments (12–14). The ECM of both species, however, contain many proteins other than those comprising pili,

including a number of *c*-type cytochromes, and their contributions to extracellular electron transport have not been determined under physiologically relevant conditions owing largely to the lack of information regarding their spatial organization. Recently, it has been proposed that microbes inhabiting marine sediments may use a network of such filaments and other extracellular proteins to couple oxidation of sulfide in anoxic sediment with reduction of oxygen in overlying oxic sediment, resulting in the transport of electrons over centimeter-scale distances (15).

Geobacter as a Model System for Studying Micrometer-Scale Biological Electron Transport

Geobacter spp. are microorganisms that inhabit subsurface environments, such as marine sediments (16), and they are widely studied for their distinct ability to acquire energy by coupling intracellular oxidation of organic matter, such as acetate, with extracellular electron transfer to insoluble (i.e., mineral) electron acceptors (17). *Geobacter* are also able to directly transfer electrons to noncorrosive anodes of electrochemical reactors, resulting in electrical current coupled to metabolic organic matter oxidation (18). When grown using an anode as their metabolic electron acceptor, *Geobacter* cells adhere to the anode surface, proliferate, and form a persistent multimicrobe-thick biofilm in which all cells comprising the biofilm appear to contribute to current generation (19–21). Such biofilms are electrically conductive, inferred by the ability of cells not in direct contact with the anode surface to contribute to current generation (22), and confirmed by two-electrode conductivity measurements (20, 23). *Geobacter* cells possess an abundance of multiheme *c*-type cytochromes on their outer membrane, in the ECM, and along PilA-pili (24–33). Cyclic voltammetry (19, 34–37) and spectroelectrochemical measurements (38–43) of actively respiring *Geobacter* biofilms are consistent with long-range electron transport mediated by sequential electron transfer reactions through a network of bound redox cofactors comprised of ECM *c*-type cytochromes terminating with electron transfer to the anode surface. This proposed process, analogous to diffusive electron transport observed for redox polymers containing discrete redox moieties (20, 44–48), is an extension of the normal mode of electron transport in biological systems involving redox proteins (2) to longer length scales (up to 18 µm in the case of biofilms described here).

The ability of a *Geobacter* biofilm to use an electrode as its terminal metabolic electron acceptor allows precise measurement of the rate of extracellular electron transport to the anode as current and enables modulation of the rate and driving force for extracellular electron transport by external control of the electrode potential. This ability enables application of electrochemical techniques, such as cyclic voltammetry (19, 20) and

MICROBIOLOGY

CHEMISTRY

chronoamperometry (49–51), and combined with availability of its genome sequence and genetic system (52), it makes possible the investigation of the mechanism of extracellular electron transport to a degree not yet possible with non-electrode-using systems. Understanding the processes that govern long-range biofilm electron transport from cells comprising a biofilm to the underlying anode surface has important implications for optimization of microbe-catalyzed electrode reactions, such as anode-coupled oxidation of organic matter for wastewater treatment and energy transformation (53–57) and cathode-coupled reduction of carbon dioxide to liquid fuel precursors (58, 59) in microbial fuel cells and microbial electrolysis cells. It may also provide valuable insights into the mechanism of long-range biological electron transport in environmental processes not involving electrodes.

A Redox Gradient Is Expected to Accompany Multistep Electron Hopping

A predicted feature of long-range multistep electron hopping is the presence of a redox gradient, in which the local oxidation state of the biofilm decreases with increasing distance from the anode surface (14) (that is, the local concentration of electrons residing in biofilm cofactors is expected to be higher farther from the anode surface). This gradient is expected to result from reduction of cofactors by cells distributed across the biofilm coupled to cellular oxidation of organic matter and oxidation of cofactors at the anode surface, where the potential applied to the anode determines the local oxidation state of the biofilm in the vicinity of the anode surface. This gradient is also expected to provide the driving force for electron transport as occurs for redox polymers (44), in which electrons effectively diffuse from areas of high to low concentration (from cells to the anode surface) by electron transfer among cofactors.

Here, we provide experimental evidence for the existence of an intrabiofilm redox gradient within actively respiring *G. sulfurreducens* WT biofilms. Furthermore, the magnitude of the gradient seems to correlate with catalytic current coupled to acetate oxidation in response to changing potential applied to the anode in a manner consistent with multistep electron hopping. In addition, we provide additional experimental evidence indicating that electron transport through an actively respiring *Geobacter* biofilm between two electrodes acting as an electron source and drain results from generation of a redox gradient between the electrodes in response to the potentials applied to the electrodes. The magnitude of the gradient seems to depend on the electrode potentials in a manner also consistent with multistep electron hopping (20). In these source-drain measurements, electron transport is not coupled to acetate oxidation, but rather, the more negative electrode (the source) supplies the electrons that are conducted through the biofilm to the more positive electrode (the drain). Comparison of measurements of biofilm electron transport to an anode coupled to acetate oxidation with measurements of biofilm electron transport between a source and drain not coupled to acetate oxidation indicates that *Geobacter* biofilms seem to contain a number of cofactors able to participate in multistep electron hopping. The majority, however, do not seem able to participate in electron transport coupled to acetate oxidation, because the formal potentials are too negative to accept electrons originating from acetate.

Results

Biofilm-Modified Interdigitated Microelectrode Arrays. Fig. 1 depicts an SEM image of a *G. sulfurreducens* WT biofilm grown on a gold interdigitated microelectrode array (IDA), an electrode configuration developed to study conductive properties of polymer films (60). IDAs used here are comprised of 100 parallel 15-μm-wide × 0.48-cm-long gold microelectrode bands patterned onto a glass slide separated by 15-μm-wide gaps. Every other band is electrically connected at two opposite edges of the array, forming two interdigitated electrodes (electrode 1 and electrode 2), each comprised of 50 microelectrode bands, effectively separated by a single 15-μm-wide × 48-cm-long single serpentine-shaped gap (Fig. 1, *Inset*). The biofilm was grown by poising both
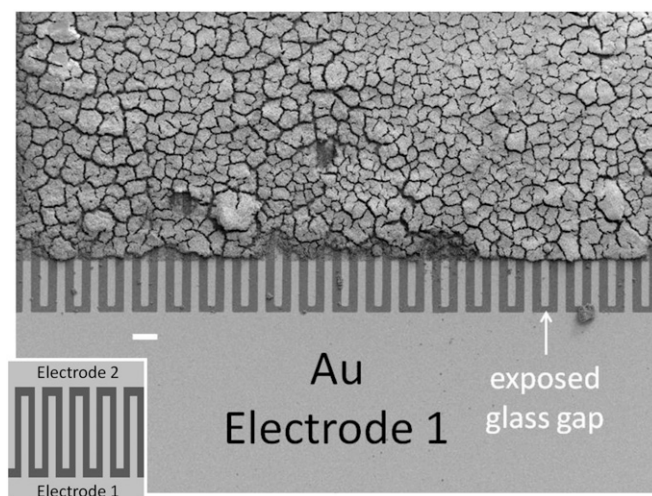

Fig. 1. SEM of a fully grown WT *G. sulfurreducens* biofilm grown on a gold interdigitated microelectrode array (IDA). The edges of the array were masked with photoresist, defining the electroactive area where the biofilm grew, which was removed during preparation for SEM imaging. An unmasked edge of the array is shown at the bottom, where alternate microelectrode bands comprising electrode 1 are electrically connected. (Scale bar: 45 μm.) (*Inset*) Schematic representation of a portion of the IDA depicting 10 of 100 microelectrode bands (not to scale; dimensions provided in the text).

electrodes as anodes at +0.300 V vs. Ag/AgCl [approximately +0.500 V vs. standard hydrogen electrode (SHE)] in media containing excess acetate (10 mM) until a self-determined limiting catalytic current of 50 μA (25 μA for each electrode) was achieved, corresponding to a biofilm thickness of 18 μm, on average, that was sufficiently thick to span the gap between adjacent interdigitated microelectrode bands (*SI Materials and Methods*). Two types of electrochemical measurements performed on actively respiring *G. sulfurreducens* WT biofilms grown on IDAs are presented here after the biofilms were first grown using both electrodes as anodes. In the first type (Fig. 2*A*), a potential is applied only to electrode 1, which continues to act as an anode, whereas electrode 2 is at open circuit and monitors the local oxidation state of the biofilm in the vicinity of electrode 2 while electron transport through the biofilm to electrode 1 coupled to acetate oxidation is occurring. In the second type (electrochemical gate measurements) (Fig. 2*B*), different potentials are applied to electrodes 1 and 2, which act as an electron drain and source while maintaining a constant potential difference between the electrodes inducing electron transport between the electrodes through the intervening biofilm that is not coupled to acetate oxidation.

Evidence for a Biofilm Redox Gradient During Catalytic Current Generation. Fig. 3*A* depicts catalytic (turnover) cyclic voltammetry (CV) recorded for electrode 1 while electrode 2 was at open circuit (Fig. 2*A*). Here, only the set of microelectrode bands comprising electrode 1 was used to collect electrons resulting from acetate oxidation. The CV exhibits the sigmoid-shape dependency of steady state catalytic current on applied potential reported for full grown *G. sulfurreducens* biofilms (19, 20, 36), consistent with an electrode catalytic (EC) reaction scheme (61), in which a reactant (in this case, acetate) that cannot be directly oxidized by an electrode owing to poor kinetics is coupled to reduction of a redox cofactor that can be reversibly oxidized by an electrode, such as a *c*-type cytochrome (41). The negative deviation in current observed during the anodic scan of the experimental CV has been previously noted, and it is attributed to possible inhibition of acetate oxidation and/or possible accumulation of electrons in cells occurring at the end of the cathodic scan and beginning of the anodic scan, when the potential applied to electrode 1 was fairly negative (20). Fig. 3*A*, *Inset* depicts nonturnover CV (recorded in the absence of acetate),
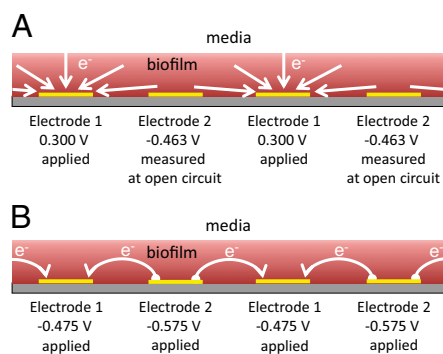
Fig. 2. Schematic depiction of a cross-section of biofilm-coated IDA. (A) Anode/open circuit experiment in which electrode 1 is used as an anode that collects electrons coupled to cellular oxidation of acetate throughout the biofilm, whereas electrode 2 is at open circuit and therefore, does not accept electrons; however, it is used to measure oxidation state of the biofilm in the vicinity of electrode 2. White arrows indicate flux of the electrons to microelectrode bands comprising electrode 1 coupled to cellular oxidation of acetate throughout the biofilm continuously supplied by diffusion from adjacent media. A specific case is shown, in which the potential applied to electrode 1 is +0.300 V and the open circuit potential measured at electrode 2 is –0.463 V based on the results depicted in Fig. 3B. In this case, while the biofilm is fully oxidized in vicinity of electrode 1, it is only 44% oxidized in vicinity of electrode 2 (Fig. 3B). (B) Electrochemical gate experiment in which different potentials are applied to electrodes 1 and 2 while maintaining a constant potential offset between the electrodes, resulting in electron transport through the biofilm from the more negative electrode (electron source is electrode 2) to the more positive electrode (electron drain is Electron 1), which is indicated by white arrows. A specific case is shown, in which the potential applied to electrode 1 is –0.475 V and the potential applied to electrode 2 is –0.575 V, resulting in the largest conducted current based on the results depicted in Fig. 5A. Unless otherwise noted, potentials are vs. Ag/AgCl.

where current is attributed to changing the oxidation state of redox cofactors in the biofilm (i.e., pseudocapacitance) (19, 39, 40) and multiple voltammetric peaks indicate possible presence of multiple redox cofactors spanning a range in formal potentials. Overlaid on to the cathodic voltammetric scan are fits based on Eq. **1** derived by modeling catalytic current generation by a *Geobacter* biofilm as an EC reaction scheme (61), in which electron transport occurs by multistep electron hopping (20) (Eq. **1**):

$$i_{cat} = i_L (X_{Ox})_{z=0,1}. \tag{1}$$

Here, steady catalytic current measured at electrode 1 coupled to biofilm acetate oxidation, i_{cat}, scales in proportion to the local biofilm oxidation state in the vicinity of electrode 1, $(X_{Ox})_{z=0,1}$ (portion of cofactors that directly exchange electrons with electrode 1 that are in the oxidized form where z is distance from the electrode surface), and the maximum catalytic current, i_L (Fig. 3A, 39.3 µA), which occurs when $(X_{Ox})_{z=0,1} = 1$. i_L is dependent on the IDA geometry, growth state of the biofilm (19), concentration of redox cofactors in the biofilm, and rate constant for electron exchange between adjacent cofactors (14). If electron exchange between electrode 1 and cofactors at the electrode surface is fast (20), then $(X_{Ox})_{z=0,1}$ can be determined from the potential applied to electrode 1, E_1, by a modified version of the Nernst Equation (Eq. **2**):

$$(X_{Ox})_{z=0,j} = \frac{\exp\left[g\dfrac{nF}{RT}\left(E_j - (E^{o'})_{avg}\right)\right]}{1 + \exp\left[g\dfrac{nF}{RT}\left(E_j - (E^{o'})_{avg}\right)\right]}. \tag{2}$$

$j = 1$ indicates electrode 1, where $(E^{o'})_{avg}$ is the weighted average of formal potentials of cofactors that participate in multistep electron hopping, n is the number of electrons transferred at a time between a cofactor and electrode 1 ($n = 1$) (36), and F, R,

and T (303 K) have their standard meanings. g is an empirical factor invoked here to describe the degree of heterogeneity among cofactors with respect to formal potential. When $g = 1$, all of the cofactors have the same formal potential, and a smaller value of g indicates greater heterogeneity among cofactors, resulting in a wider potential range, over which the oxidation state of the biofilm in the vicinity of the electrode surface changes from being fully oxidized to fully reduced (14, 62).
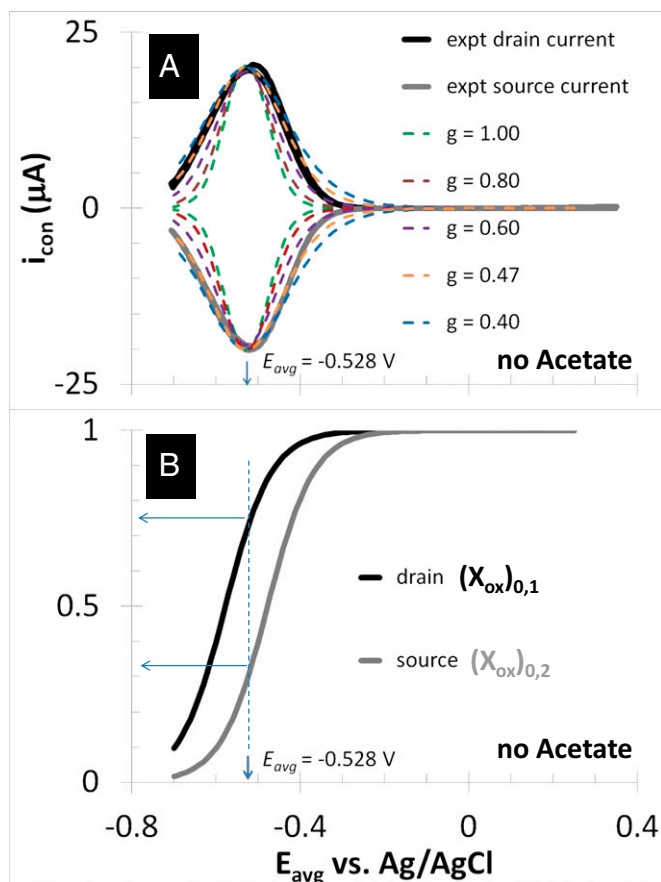
In Fig. 3A, the best fit of the experimental CV to Eq. **1** based on matching the shape and midpoint potential (potential at which $i_{cat} = i_L/2$; E_M in Fig. 3A) is observed for $(E^{o'})_{avg} = -0.458 \pm 0.0025$ V vs. Ag/AgCl and $g = 0.80 \pm 0.1$, consistent with non-negligible heterogeneity among biofilm cofactors involved in multistep electron hopping during catalytic current generation when current is coupled to biofilm acetate oxidation. Fig. 3B depicts the concomitantly measured open circuit potential for electrode 2, E_2, which did not collect electrons since at open circuit, but varied in time in response to E_1. Here, E_2 reflects the oxidation state of redox cofactors in the vicinity of electrode 2, $(X_{Ox})_{z=0,2}$. For example, when $E_1 > -0.3$ V, for which $i_{cat} = i_L$, then $E_2 = -0.463$ V, indicating that redox cofactors in the vicinity of electrode 2 are partially reduced based on Fig. 3A (*Inset*), although they are fully oxidized in the vicinity of electrode 1 (40). If electron exchange between redox cofactors and electrode 2 is fast, then $(X_{Ox})_{z=0,2}$ can also be determined from Eq. **2** ($j = 2$) for each value of E_2. Fig. 3B also depicts $(X_{Ox})_{z=0,1}$ and $(X_{Ox})_{z=0,2}$
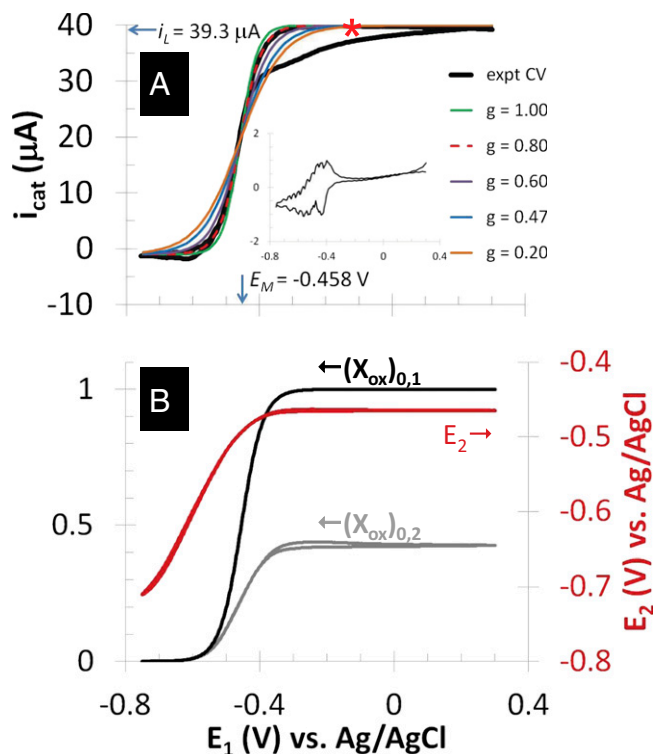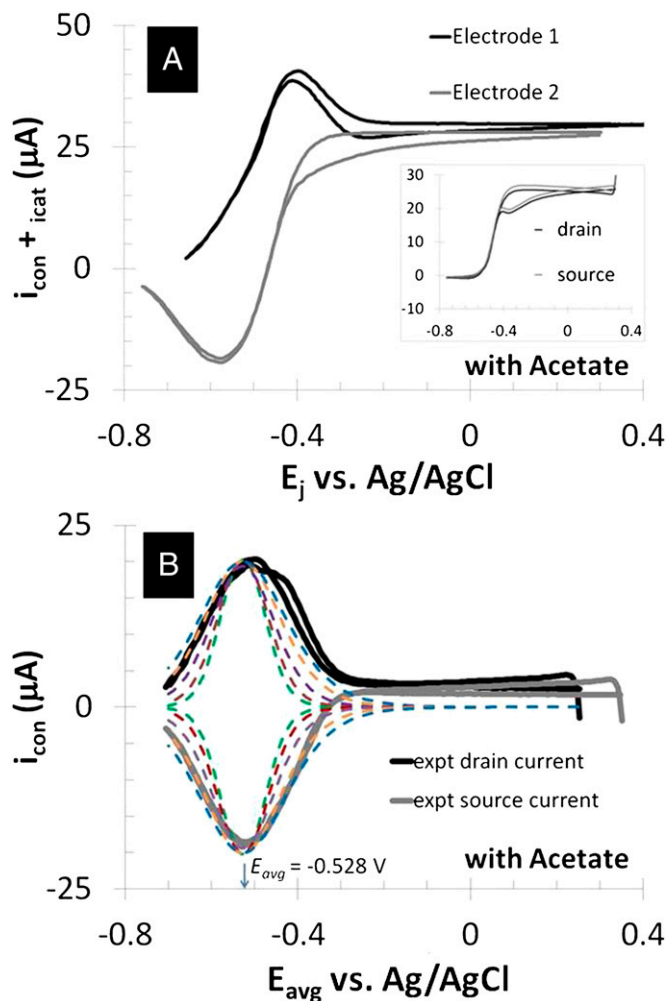

Fig. 3. Anode/open circuit experiment. (A) Catalytic (turnover) CV recorded by scanning potential of electrode 1 at 0.002 V/s from +0.300 V to –0.750 V (cathodic scan) and back to +0.300 V (anodic scan), whereas electrode 2 is at open circuit (asterisk indicates cathodic scan). Catalytic current, i_{cat}, results from the electron transport to microelectrode bands comprising electrode 1 coupled to cellular acetate oxidation throughout the biofilm. The x axis corresponds to the potential applied to electrode 1. Fits are based on Eq. **1**. (A, Inset) Nonturnover CV of electrode 1 at 0.002 V/s recorded in absence of acetate, revealing voltammetric peaks attributable to biofilm redox cofactors (same axis scales). (B, right axis) Potential measured for electrode 2 vs. potential applied to electrode 1. (B, left axis) Corresponding biofilm oxidation state in the vicinity of electrode 1, $(X_{Ox})_{z=0,1}$, and electrode 2, $(X_{Ox})_{z=0,2}$, vs. potential applied to electrode 1 calculated using Eq. **2**.

calculated using Eq. **2** from E_1 (applied to electrode 1) and E_2 (measured at electrode 2) vs. E_1 using values for $(E^{o'})_{avg}$ and g determined from Fig. 3*A*. Comparison of Fig. 3*A* with *B* reveals that, for all instances in which catalytic current occurs, $(X_{Ox})_{z=0,1}$ is higher than $(X_{Ox})_{z=0,2}$, indicative of a redox gradient extending across the gap separating adjacent microelectrode bands (i.e., the effective concentration of electrons residing in cofactors in the vicinity of electrode 2 is higher than in the vicinity of electrode 1). Furthermore, increasing catalytic current coincides with increasing difference between $(X_{Ox})_{z=0,1}$ and $(X_{Ox})_{z=0,2}$, and the maximum catalytic current coincides with the maximum difference between these values, consistent with electron transport to electrode 1 during catalytic current generation that is redox gradient-driven. It is important to note the lack of a negative deviation in E_2 and therefore, $(X_{Ox})_{z=0,2}$ observed during the anodic voltammetric scan as observed for i_{cat}, indicating that the negative deviation observed for i_{cat} appears not to be associated with extracellular electron transport.

Evidence for a Biofilm Redox Gradient Using Electrochemical Gate Measurements. Figs. 4 and 5 depict results of experiments in which potentials are applied to both electrodes that are changed in unison while maintaining a constant 0.1 V offset between them (i.e., electrochemical gate measurements) (60), where the different electrode potentials establish different values for $(X_{Ox})_{z=0,1}$ and $(X_{Ox})_{z=0,2}$. Fig. 4*A* depicts dependency of the resulting

Fig. 5. Electrochemical gate experiment recorded under turnover condition (with acetate present). (*A*) Because each electrode also acts as an anode, the resulting current measured at electrode 1 (drain) is the sum of catalytic current and conducted current out of the biofilm, and at electrode 2 (source) is the sum of catalytic current and conducted current into the biofilm, plotted here vs. potential applied to each electrode. Electrode potentials were scanned at 0.002 V/s while maintaining electrode 2 at a fixed −0.100 V offset vs. electrode 1. (*A, Inset*) CV recorded for the two electrodes simultaneously without an offset such that $i_{con} = 0$ for background subtraction of i_{cat} for each of electrode (same axis scales). (*B*) i_{con} vs. E_{avg} after background subtracting i_{cat}. Qualitative fits are based on Eq. **3** (same as in Fig. 4*A*).

Fig. 4. Electrochemical gate experiment recorded under nonturnover condition (no acetate present). (*A*) Conducted current, i_{con}, vs. average potential applied to electrodes 1 and 2, E_{avg}. Electrode potentials were scanned at 0.002 V/s while maintaining electrode 2 (electron source) at a fixed −0.100 V offset vs. electrode 1 (electron drain). Fits are based on Eq. **3**. (*B*) The corresponding plot of $(X_{Ox})_{z=0,1}$ and $(X_{Ox})_{z=0,2}$ vs. E_{avg} was calculated using Eq. **2**. Arrows indicate the condition when difference between $(X_{Ox})_{z=0,1}$ and $(X_{Ox})_{z=0,2}$ is the greatest, resulting in the largest value of i_{con}.

conducted current, i_{con}, recorded under nonturnover condition after acetate removal to the average of the potentials applied to the electrodes, $E_{avg} = (E_1 + E_2)/2$. Here, current was measured at both electrodes, where negative current indicates electron transfer from the more negative electrode (electrode 2, electron source) into the biofilm, whereas positive current, as in the case of an anode, indicates electron transfer out of the biofilm to the more positive electrode (electrode 1, electron drain). The magnitude of current measured at either electrode, i_{con}, is attributed to electron transport through the biofilm between adjacent microelectrode bands comprising electrodes 1 and 2 that is not coupled to acetate oxidation. Comparison of Fig. 4*A* with Fig. 3*A* (*Inset*) indicates that current due to pseudocapacitance is a negligible contribution to i_{con}. Depicted in Fig. 4*A* are fits to i_{con} vs. E_{avg} based on Eq. **3**,

$$i_{con} = i_M \left[(X_{Ox})_{z=0,1} - (X_{Ox})_{z=0,2} \right],$$ [3]

that follows directly from equation 21 in the work by Strycharz-Glaven et al. (14, 63), which is based on multistep electron hopping. Here i_M is the maximum current that can be conducted through the biofilm that is dependent on the same parameters as i_L. The condition at which $i_{con} = i_M$ can occur is when $(X_{Ox})_{z=0,1} = 1$ and $(X_{Ox})_{z=0,2} = 0$, the condition at which the magnitude of the redox gradient between adjacent microelectrode bands is maximized (44). The best fits based on peak potential and peak width at one-half height are obtained for $E_{avg} = -0.528 \pm 0.0025$ V and $g = 0.47 \pm 0.01$, indicating that redox mediators involved in generation of i_{con} by multistep electron hopping are considerably more heterogeneous and have a considerably more negative average formal potential than redox cofactors involved in generation of i_{cat}. Previous modeling (20) indicates that redox cofactors involved in generation of i_{cat} cannot have formal potentials that are more negative than the midpoint potential of the catalytic CV (E_M, -0.458 ± 0.0025 V vs. Ag/AgCl) (Fig. 3A), which is ultimately constrained by the oxidation potential of acetate (-0.49 V vs. Ag/AgCl). As such, the majority of redox cofactors able to participate in multistep electron hopping not coupled to acetate oxidation resulting in i_{con} cannot participate in multistep electron hopping that is coupled to acetate oxidation resulting in i_{cat}, because the supply of electrons during i_{con} generation is not constrained in potential [that is, the source electrode can supply electrons into the biofilm with higher potential energy (at a more negative potential) than those electrons originating from acetate oxidation].

Fig. 4B depicts the dependency of $(X_{Ox})_{z=0,1}$ and $(X_{Ox})_{z=0,2}$ on E_{avg} determined from Eq. **2** using the best-fit parameters from Fig. 4A. As expected for redox gradient-driven electron transport, an appreciable i_{con} occurs only when there is an appreciable difference between $(X_{Ox})_{z=0,1}$ and $(X_{Ox})_{z=0,2}$, and the largest i_{con} coincides with the largest difference in these values (44, 60). Calculated values of $(X_{Ox})_{z=0,1}$ and $(X_{Ox})_{z=0,2}$ based on Eq. **2**, for which i_{con} is largest, are 0.32 and 0.74, respectively, the largest difference between these values that can be achieved given the 0.100 V offset maintained between the electrodes ($E_1 = -0.478$ V, $E_2 = -0.578$ V) for $g = 0.47$.

Fig. 5A depicts results of measurements performed in an identical manner as those measurements depicted in Fig. 4A but under turnover condition. When acetate is present, i_{con} is superimposed onto i_{cat} (Fig. 5B), because each electrode also acts as an anode. To a first approximation, i_{cat} can be background subtracted using CV, in which the potentials of both electrodes are changed in unison with no potential offset between them, resulting in only i_{cat} at each of the electrodes (Fig. 5A, Inset). Fig. 5B depicts results of this subtraction process, where the residual i_{cat} observed results presumably from competition among cofactors in electron transport associated with i_{cat} and i_{con}. Regardless, Fig. 5B indicates that i_{con} depends on the potentials applied to both electrodes in nearly the same manner when acetate is present, suggesting that i_{cat} may be localized to a relatively small portion of the biofilm directly between adjacent microelectrode bands.

Discussion

Two types of electrochemical measurements performed on *G. sulfurreducens* WT biofilms grown on IDAs are presented here. In the first type, a potential is applied only to electrode 1, which continues to act as an anode. The applied potential directly determines the local oxidation state of the biofilm in the vicinity of electrode 1. In contrast, electrode 2 is at open circuit, such that its potential reflects the local oxidation state of the biofilm in the vicinity of electrode 2 that is indirectly influenced by the potential applied to electrode 1. The difference in the electrode potentials when catalytic current is generated at electrode 1 is interpreted to reflect a difference in local oxidation state of the biofilm in the vicinity of each of the electrodes, indicating

the presence of redox gradient that drives electron transport through the biofilm to electrode 1 when such electron transport is coupled to cellular acetate oxidation. In the second type (electrochemical gate measurements), different potentials are applied to electrodes 1 and 2, which act as an electron drain and source, respectively, while maintaining a constant potential difference between the electrodes. The applied potentials directly determine the local oxidation state of the biofilm in the vicinity of each of the electrodes. The resulting current conducted through the biofilm between the electrodes is interpreted to reflect generation of redox gradient between the electrodes in response to the applied potentials that is not coupled to acetate oxidation.

As shown here for a living, actively respiring *G. sulfurreducens* WT biofilm, electrochemical gate measurements result in a completely reversible current peak spanning the formal potentials of biofilm redox cofactors as observed for redox polymers known to engage in multistep electron hopping (60). The peak in conducted current lies more negative than expected based on the midpoint potential of the catalytic current-potential dependency (Fig. 3A), and it is broader than expected for a single type of redox cofactor, suggesting that multiple types of redox cofactors possessing different oxidation potentials can be accessed by electrons driven by the conducting current, i_{con}, that are not involved in catalytic current generation, i_{cat} (39, 40). WT *G. sulfurreducens* contains genes encoding for more than 50 multiheme cytochromes (64) in addition to those cytochromes identified to be important in establishing biofilms grown on anodes (36, 65); therefore, it is not surprising that some of them can pass electrons but are not recruited for catalytic current.

Implications

The results of our electrochemical gate measurements directly contradict results recently reported in the work by Malvankar et al. (23), which attributes long-range electron transport through *Geobacter* biofilms not to multistep electron hopping but to an intrinsic "metallic-like" conductivity of PilA-pili (23). According to their model, however, the current–potential dependency depicted in Figs. 4A and 5A should be sigmoid-shaped and not peaked-shaped (63). The nature of *Geobacter* biofilm conductivity is contested because of a lack of direct evidence for cytochrome spatial distribution within the biofilm ECM or direct structural evidence for the proposed conductive PilA-pili conclusively supporting either a model for multistep electron hopping or metallic-like conductivity model (21, 66–67). Because of the role of PilA-pili in biofilm formation (22) as well as cytochrome secretion (9, 52) and extracellular localization (32), we subscribe to the supposition that PilA-pili are important for *Geobacter* biofilm structure and cytochrome organization (52), and like in other biological systems (2), redox proteins are the primary charge carriers. The results also raise questions regarding the thermodynamics of electron transport through such biofilms.

Materials and Methods

IDAs were fabricated in house using standard procedures. Two electrode experiments were performed under anaerobic conditions (80:20 N_2:CO_2) using a biopotentiostat (AFCBP1; Pine Instruments), counterelectrode (graphite rod), and reference electrode (Ag/AgCl, 3 M KCl; CH Instruments) in freshwater medium. *G. sulfurreducens* strain DL1 (51573; ATCC) was maintained in freshwater media containing 40 mM fumarate and 10 mM sodium acetate as described previously (14, 20, 68, 69). Electrochemical cells containing 10 mM acetate were inoculated with log-phase *G. sulfurreducens* strain DL1 (3% vol/vol inoculum, OD = 0.4–0.6; 51573; ATCC), while IDA electrodes 1 and 2 were maintained at +0.300 V vs. Ag/AgCl. Details of the experimental procedures are provided in *SI Materials and Methods*.

1. Gray HB, Winkler JR (2010) Electron flow through metalloproteins. *Biochim Biophys Acta* 1797:1563–1572.
2. Gray HB, Winkler JR (1996) Electron transfer in proteins. *Annu Rev Biochem* 65:537–561.
3. Gralnick JA, Newman DK (2007) Extracellular respiration. *Mol Microbiol* 65(1):1–11.
4. Hartshorne RS, et al. (2009) Characterization of an electron conduit between bacteria and the extracellular environment. *Proc Natl Acad Sci USA* 106:22169–22174.

Snider et al.

MICROBIOLOGY

CHEMISTRY

5. Hartshorne RS, et al. (2007) Characterization of Shewanella oneidensis MtrC: A cell-surface decaheme cytochrome involved in respiratory electron transport to extracellular electron acceptors. *J Biol Inorg Chem* 12:1083–1094.

6. Clarke TA, et al. (2011) Structure of a bacterial cell surface decaheme electron conduit. *Proc Natl Acad Sci USA* 108:9384–9389.

7. Reguera G, et al. (2005) Extracellular electron transfer via microbial nanowires. *Nature* 435:1098–1101.

8. Summers ZM, et al. (2010) Direct exchange of electrons within aggregates of an evolved syntrophic coculture of anaerobic bacteria. *Science* 330:1413–1415.

9. Cologgi DL, Lampa-Pastirk S, Speers AM, Kelly SD, Reguera G (2011) Extracellular reduction of uranium via Geobacter conductive pili as a protective cellular mechanism. *Proc Natl Acad Sci USA* 108:15248–15252.

10. El-Naggar MY, et al. (2010) Electrical transport along bacterial nanowires from Shewanella oneidensis MR-1. *Proc Natl Acad Sci USA* 107:18127–18131.

11. El-Naggar MY, Gorby YA, Xia W, Nealson KH (2008) The molecular density of states in bacterial nanowires. *Biophys J* 95:L10–L12.

12. Pirbadian S, El-Naggar MY (2012) Multistep hopping and extracellular charge transfer in microbial redox chains. *Phys Chem Chem Phys*, 10.1039/C2CP41185G.

13. Polizzi NF, Skourtis SS, Beratan DN (2012) Physical constraints on charge transport through bacterial nanowires. *Faraday Discuss* 155:43–62.

14. Strycharz-Glaven SM, Snider RM, Guiseppi-Elie A, Tender LM (2011) On the electrical conductivity of microbial nanowires and biofilms. *Energy Environ Sci* 4:4366–4379.

15. Nielsen LP, Risgaard-Petersen N, Fossing H, Christensen PB, Sayama M (2010) Electric currents couple spatially separated biogeochemical processes in marine sediment. *Nature* 463:1071–1074.

16. Lovley DR, et al. (2011) Geobacter: The microbe electric's physiology, ecology, and practical applications. *Advances in Microbial Physiology*, ed Robert KP (Academic, London), Vol 59, pp 1–100.

17. Nevin KP, Lovley DR (2000) Lack of production of electron-shuttling compounds or solubilization of Fe(III) during reduction of insoluble Fe(III) oxide by Geobacter metallireducens. *Appl Environ Microbiol* 66:2248–2251.

18. Bond DR, Holmes DE, Tender LM, Lovley DR (2002) Electrode-reducing microorganisms that harvest energy from marine sediments. *Science* 295:483–485.

19. Strycharz-Glaven SM, Tender LM (2012) Study of the mechanism of catalytic activity of G. sulfurreducens biofilm anodes during biofilm growth. *ChemSusChem* 5:1106–1118.

20. Strycharz SM, et al. (2011) Application of cyclic voltammetry to investigate enhanced catalytic current generation by biofilm-modified anodes of Geobacter sulfurreducens strain DL1 vs. variant strain KN400. *Energy Environ Sci* 4:896–913.

21. Bond DR, Strycharz-Glaven SM, Tender LM, Torres CI (2012) On electron transport through Geobacter biofilms. *ChemSusChem* 5:1099–1105.

22. Reguera G, et al. (2006) Biofilm and nanowire production leads to increased current in Geobacter sulfurreducens fuel cells. *Appl Environ Microbiol* 72:7345–7348.

23. Malvankar NS, et al. (2011) Tunable metallic-like conductivity in microbial nanowire networks. *Nat Nanotechnol* 6:573–579.

24. Ding YHR, et al. (2006) The proteome of dissimilatory metal-reducing microorganism Geobacter sulfurreducens under various growth conditions. *Biochim Biophys Acta* 1764:1198–1206.

25. Ding YHR, et al. (2008) Proteome of Geobacter sulfurreducens grown with Fe(III) oxide or Fe(III) citrate as the electron acceptor. *Biochim Biophys Acta* 1784:1935–1941.

26. Leang C, Coppi MV, Lovley DR (2003) OmcB, a c-type polyheme cytochrome, involved in Fe(III) reduction in Geobacter sulfurreducens. *J Bacteriol* 185:2096–2103.

27. Mehta T, Coppi MV, Childers SE, Lovley DR (2005) Outer membrane c-type cytochromes required for Fe(III) and Mn(IV) oxide reduction in Geobacter sulfurreducens. *Appl Environ Microbiol* 71:8634–8641.

28. Qian XL, Reguera G, Mester T, Lovley DR (2007) Evidence that OmcB and OmpB of Geobacter sulfurreducens are outer membrane surface proteins. *FEMS Microbiol Lett* 277:21–27.

29. Inoue K, et al. (2010) Purification and characterization of OmcZ, an outer-surface, octaheme c-type cytochrome essential for optimal current production by Geobacter sulfurreducens. *Appl Environ Microbiol* 76:3999–4007.

30. Inoue K, et al. (2011) Specific localization of the c-type cytochrome OmcZ at the anode surface in current-producing biofilms of Geobacter sulfurreducens. *Environ Microbiol Rep* 3:211–217.

31. Rollefson JB, Stephen CS, Tien M, Bond DR (2011) Identification of an extracellular polysaccharide network essential for cytochrome anchoring and biofilm formation in Geobacter sulfurreducens. *J Bacteriol* 193:1023–1033.

32. Leang C, Qian X, Mester T, Lovley DR (2010) Alignment of the c-type cytochrome OmcS along pili of Geobacter sulfurreducens. *Appl Environ Microbiol* 76:4080–4084.

33. Qian X, et al. (2011) Biochemical characterization of purified OmcS, a c-type cytochrome required for insoluble Fe(III) reduction in Geobacter sulfurreducens. *Biochim Biophys Acta* 1807:404–412.

34. Fricke K, Harnisch F, Schröder U (2008) On the use of cyclic voltammetry for the study of anodic electron transfer in microbial fuel cells. *Energy Environ Sci* 1:144–147.

35. Srikanth S, Marsili E, Flickinger MC, Bond DR (2008) Electrochemical characterization of Geobacter sulfurreducens cells immobilized on graphite paper electrodes. *Biotechnol Bioeng* 99:1065–1073.

36. Richter H, et al. (2009) Cyclic voltammetry of biofilms of wild type and mutant Geobacter sulfurreducens on fuel cell anodes indicates possible roles of OmcB, OmcZ, type IV pili, and protons in extracellular electron transfer. *Energy Environ Sci* 2:506–516.

37. Marsili E, Sun J, Bond DR (2010) Voltammetry and growth physiology of Geobacter sulfurreducens biofilms as a function of growth stage and imposed potential. *Electroanalysis* 22:865–874.

38. Jain A, Gazzola G, Panzera A, Zanoni M, Marsili E (2011) Visible spectroelectrochemical characterization of Geobacter sulfurreducens biofilms on optically transparent indium tin oxide electrode. *Electrochim Acta* 56:10776–10785.

39. Liu Y, Kim H, Franklin RR, Bond DR (2011) Linking spectral and electrochemical analysis to monitor c-type cytochrome redox status in living Geobacter sulfurreducens biofilms. *ChemPhysChem* 12:2235–2241.

40. Liu Y, Bond DR (2012) Long-distance electron transfer by G. sulfurreducens biofilms results in accumulation of reduced c-type cytochromes. *ChemSusChem* 5:1047–1053.

41. Millo D, et al. (2011) In situ spectroelectrochemical investigation of electrocatalytic microbial biofilms by surface-enhanced resonance Raman spectroscopy. *Angew Chem Int Ed Engl* 50:2625–2627.

42. Busalmen JP, Esteve-Nuñez A, Berná A, Feliu JM (2010) ATR-SEIRAs characterization of surface redox processes in G. sulfurreducens. *Bioelectrochemistry* 78:25–29.

43. Virdis B, Harnisch F, Batstone DJ, Rabaey K, Donose BC (2012) Non-invasive characterization of electrochemically active microbial biofilms using confocal Raman microscopy. *Energy Environ Sci* 5:7017–7024.

44. Dalton EF, et al. (1990) Charge transport in electroactive polymers consisting of fixed molecular redox sites. *Chem Phys* 141:143–157.

45. Katakis I, Heller A (1992) L-alpha-glycerophosphate and L-lactate electrodes based on the electrochemical "wiring" of oxidases. *Anal Chem* 64:1008–1013.

46. Forster RJ, Walsh DA, Mano N, Mao F, Heller A (2004) Modulating the redox properties of an osmium-containing metallopolymer through the supporting electrolyte and cross-linking. *Langmuir* 20:862–868.

47. Heller A (1992) Electrical connection of enzyme redox centers to electrodes. *J Phys Chem* 96:3579–3587.

48. Hodak J, Etchenique R, Calvo EJ, Singhal K, Bartlett PN (1997) Layer-by-layer self-assembly of glucose oxidase with a poly(allylamine)ferrocene redox mediator. *Langmuir* 13:2708–2716.

49. Schrott GD, Bonanni PS, Robuschi L, Esteve-Nuñez A, Busalmen JP (2011) Electrochemical insight into the mechanism of electron transport in biofilms of Geobacter sulfurreducens. *Electrochim Acta* 56:10791–10795.

50. Esteve-Nunez A, Busalmen JP, Berná A, Gutiérrez-Garrán C, Feliu JM (2011) Opportunities behind the unusual ability of Geobacter sulfurreducens for exocellular respiration and electricity production. *Energy Environ Sci* 4:2066–2069.

51. Bonanni PS, Schrott GD, Robuschi L, Busalmen JP (2012) Charge accumulation and electron transfer kinetics in Geobacter sulfurreducens biofilms. *Energy Environ Sci* 5:6188–6195.

52. Richter LV, Sandler SJ, Weis RM (2012) Two isoforms of Geobacter sulfurreducens PilA have distinct roles in pilus biogenesis, cytochrome localization, extracellular electron transfer, and biofilm formation. *J Bacteriol* 194:2551–2563.

53. Liu H, Ramnarayanan R, Logan BE (2004) Production of electricity during wastewater treatment using a single chamber microbial fuel cell. *Environ Sci Technol* 38:2281–2285.

54. Angenent LT, Karim K, Al-Dahhan MH, Wrenn BA, Domíguez-Espinosa R (2004) Production of bioenergy and biochemicals from industrial and agricultural wastewater. *Trends Biotechnol* 22:477–485.

55. Rozendal RA, Hamelers HVM, Rabaey K, Keller J, Buisman CJN (2008) Towards practical implementation of bioelectrochemical wastewater treatment. *Trends Biotechnol* 26:450–459.

56. Logan BE, et al. (2006) Microbial fuel cells: Methodology and technology. *Environ Sci Technol* 40:5181–5192.

57. Tender LM (2011) From mud to microbial electrode catalysts and conductive nanomaterials. *MRS Bull* 36:800–805.

58. Malik S, et al. (2009) A self-assembling self-repairing microbial photoelectrochemical solar cell. *Energy Environ Sci* 2:292–298.

59. Rabaey K, Rozendal RA (2010) Microbial electrosynthesis—revisiting the electrical route for microbial production. *Nat Rev Microbiol* 8:706–716.

60. Natan MJ, Wrighton MS (2007) Chemically modified microelectrode arrays. *Progress in Inorganic Chemistry*, ed Lippard SJ (Wiley, New York), Vol 37, pp 391–494.

61. Bard AJ, Faulkner LR (2001) *Electrochemical Methods: Fundamentals and Applications* (Wiley, New York).

62. Pickup PG, Kutner W, Leidner CR, Murray RW (1984) Redox conduction in single and bilayer films of redox polymer. *J Am Chem Soc* 106:1991–1998.

63. Malvankar NS, Tuominen MT, Lovley DR (2012) Comment on "On electrical conductivity of microbial nanowires and biofilms" by S. M. Strycharz-Glaven, R. M. Snider, A. Guiseppi-Elie and L. M. Tender, Energy Environ Sci, 2011, 4, 4366. *Energy Environ Sci* 5:6247–6249.

64. Methé BA, et al. (2003) Genome of Geobacter sulfurreducens: Metal reduction in subsurface environments. *Science* 302:1967–1969.

65. Nevin KP, et al. (2009) Anode biofilm transcriptomics reveals outer surface components essential for high density current production in Geobacter sulfurreducens fuel cells. *PLoS One* 4:e5628.

66. Strycharz-Glaven SM, Tender LM (2012) Reply to the "Comment on 'On electrical conductivity of microbial nanowires and biofilms'" by N. S. Malvankar, M. T. Tuominen and D. R. Lovley, Energy Environ. Sci., 2012, 5, DOI: 10.1039/c2ee02613a. *Energy Environ Sci* 5:6250–6255.

67. Richardson DJ, et al. (2012) The 'porin–cytochrome' model for microbe-to-mineral electron transfer. *Mol Microbiol* 85:201–212.

68. Bond DR, Lovley DR (2003) Electricity production by Geobacter sulfurreducens attached to electrodes. *Appl Environ Microbiol* 69:1548–1555.

69. Caccavo F, Jr., et al. (1994) Geobacter sulfurreducens sp. nov., a hydrogen- and acetate-oxidizing dissimilatory metal-reducing microorganism. *Appl Environ Microbiol* 60:3752–3759.